Batteries & Supercaps

Research Article
doi.org/10.1002/batt.202400509

Chemistry Europe
European Chemical Societies Publishing

www.batteries-supercaps.org

Automated Robotic Cell Fabrication Technology for Stacked-Type Lithium-Oxygen Batteries

Shoichi Matsuda,*[a, b, c] Shin Kimura,[a] and Misato Takahashi[a]

Rechargeable lithium-oxygen batteries (LOBs) are gaining interest as next-generation energy storage devices due to their superior theoretical energy density. While recent years have seen successful operation of LOBs with high cell-level energy density, the technology for cell fabrication is still in its infancy. This is because the cell fabrication procedure for LOBs is quite different from that of conventional lithium-ion batteries. The study presents a fully automated sequential robotic experimental setup for the fabrication of stacked-type LOB cells. This approach allows for high accuracy and high throughput fabrication of the cells. The developed system enables the fabrication of over 80 cells per day, which is 10 times higher than conventional human-based experiments. In addition, the high alignment accuracy during the electrode stacking and electrolyte injection process results in improved battery performance and reproducibility. The effectiveness of the developed system was also confirmed by investigating a multi-component electrolyte to maximize battery performance. We believe the methodology demonstrated in the present study is beneficial for accelerating the research and development of LOBs.

Introduction

Lithium-oxygen batteries (LOBs) are a promising candidate for next-generation energy storage devices due to their extremely high theoretical energy density.[1–4] In LOBs, metallic lithium, which has a low redox potential of −3.04 V (vs. SHE) and high theoretical capacity of 3860 mAh/g, is utilized as the active material for the negative electrode, while atmospheric oxygen is utilized for the positive electrode. For example, a theoretical energy density of 3150 Wh/kg can be achieved by multiplying an assumed operating voltage of 2.7 V with the specific capacity of 1168 mAh/g based on the reaction $2Li + O_2 = Li_2O_2$.[1] At the cell level, LOBs can achieve an energy density two to five times higher than that of Li-ion batteries. In fact, LOBs with a 500 Wh/kg energy density have already been demonstrated,[5,6] demonstrating the high energy density potential of LOBs.

While there have been numerous studies investigating materials for LOBs, such as self-standing porous carbon electrodes,[7–10] stable electrolytes,[11–16] and protective layers for lithium metal electrodes,[6,17] research on cell fabrication techniques for LOBs is still in its early stages. From a practical standpoint, multiple LOB cells must be densely stacked, similar to conventional lithium-ion batteries (LiBs), to achieve high energy density at the cell level. In stacked situations, it is necessary to have a proper cell configuration to ensure effective oxygen transfer throughout the positive electrode via the gas-diffusion layer. A 4 cm×5 cm sized 10-cell stacked LOB was fabricated and exhibited stable discharge/charge performance.[18] The effective cell area was 200 cm^2, which is 100 times larger than that of conventional coin-type cells (S = 2 cm^2). To maximize the cell-level energy density of LOBs, it is important to quantitatively control the amount of electrolyte in the porous carbon electrode. The surface of the porous carbon electrode should ideally be completely wetted with the electrolyte to enable efficient transfer of Li ions. It is crucial to maintain a balance between wetting and filling of the electrode with electrolyte. Additionally, the voids in the electrode should not be completely filled with the electrolyte to ensure oxygen transport channels from a gas diffusion layer. Several electrolyte injection techniques have been demonstrated to improve the performance of LOBs.[19] These techniques include the 'inkjet method', which uses a piezoelectric element to emit nanoliter-scale electrolyte droplets, and the 'stamping method', which uses two highly hydrophilic filters as electrolyte transfer agents to uniformly spread the electrolyte onto the carbon electrode sandwiched between them. Notably, the previous studies revealed the importance of the quality of the cell, such as inhomogeneity of electrolyte in porous carbon electrode, for maximizing the battery performance as well as the design of the cell.[20–23]

In recent years, fundamental technology related to the fabrication of practical LOB cells has been developed at the laboratory level. However, these techniques rely on human-based experiments involving manual handling of cell compo-

[a] S. Matsuda, S. Kimura, M. Takahashi
Center for Green Research on Energy and Environmental Materials, National Institute for Material Science, 1-1 Namiki, Tsukuba, Ibaraki 305-0044, Japan
E-mail: MATSUDA.Shoichi@nims.go.jp

[b] S. Matsuda
Center for Advanced Battery Collaboration, National Institute for Material Science, 1-1 Namiki, Tsukuba, Ibaraki 305-0044, Japan

[c] S. Matsuda
NIMS-SoftBank Advanced Technologies Development Center, National Institute for Material Science, 1-1 Namiki, Tsukuba, Ibaraki 305-0044, Japan

Supporting information for this article is available on the WWW under https://doi.org/10.1002/batt.202400509

Research Article
doi.org/10.1002/batt.202400509
Chemistry Europe
European Chemical Societies Publishing

nents. Therefore, a series of process technologies for handling, stacking cell components, and electrolyte injection should be developed in an automated manner. Given the differences between the current lithium-ion battery cell production process and the process required for LOB-specific cell fabrication, it is essential to establish appropriate technology. This study presents the development of an automated cell fabrication system for stacked-type LOB cells. By coordinating the operations of electrode handling, electrode stacking, and electrolyte injection processes, we have constructed a LOB cell fabrication equipment that can continuously create more than 80 LOB cells per day.

Results and Discussion

To develop an automated cell fabrication robotic system, it is important to consider the differences between LiB and LOB in the cell fabrication procedure. In conventional LiB cell fabrication, a composite electrode consisting of $LiCoO_2$ active material with binder and conductive additives coated on an aluminum metal foil is used as the positive electrode. The negative electrode utilized a composite of graphite active material with binder coated on copper metal foil. Both electrodes have a porosity of approximately 30%. A separator made of a polyolefin-based membrane with a porosity of 50% was used. The electrode materials were stacked and laminated as a pouch-type cell. The cell was then filled with electrolyte using a vacuum impregnation process. The electrolyte spreads throughout the pore space in electrodes and separators. However, it is important to note that the electrode materials and cell fabrication procedure of LOB differ significantly from those of LiB. In the case of LOB, a porous carbon membrane with a porosity of about 90% serves as the positive electrode, while a metal lithium foil is used as the negative electrode (Figure 1a). The separator is similar to that used for LiB. A membrane made of carbon fiber with a porosity of about 80% is typically used as a gas-diffusion layer. This layer functions as an oxygen transport channel from outside of the cell.

Before stacking these electrode materials, a controlled amount of electrolyte should be injected properly. This is because the void spaces in the carbon electrode and GDL should not be filled with electrolyte in order to maintain an interconnected oxygen transport pathway. Therefore, it is important to satisfy these requirements during the electrolyte injection process for LOB. Additionally, special attention should be paid to the handling of the electrodes during LOB cell fabrication. Porous carbon electrodes can become distorted when they contain electrolyte (Figures 1b and c) and can be easily damaged during electrode handling and stacking processes. Similarly, the lithium metal foil is also susceptible to damage when handled with typical ceramic-based tweezers (Figures 1d and e). To minimize damage to the electrode, the cell fabrication process should be designed to avoid handling the electrolyte after it has been injected.

Based on these considerations, we investigated the LOB cell fabrication procedure, which can be applied to an automated robotic process. The procedure is shown in Figure 2. First, the lithium metal foil with copper metal foils is transported to the cell folder. Then, the separator is also transported and stacked on top of it, and the electrolyte is injected. After that, the porous carbon-based positive electrode is also moved and placed on top of it. The proper amount of electrolyte is injected into the porous carbon-based positive electrode. The gas-diffusion layer, made of carbon fiber, is placed on top. This procedure allows for the fabrication of LOB cells with proper electrolyte injection conditions, ensuring high reproducibility while minimizing damage to the electrode materials.

We fabricated the automated LOB cell fabrication robotic system. Figure 3 showed the over-view of the automated LOB cell fabrication equipment developed in the present study. The photographic images are also shown in Figures S1 and S2. The device consists of a total of 9 parts: 5 units and 4 transport arms that connect each unit.

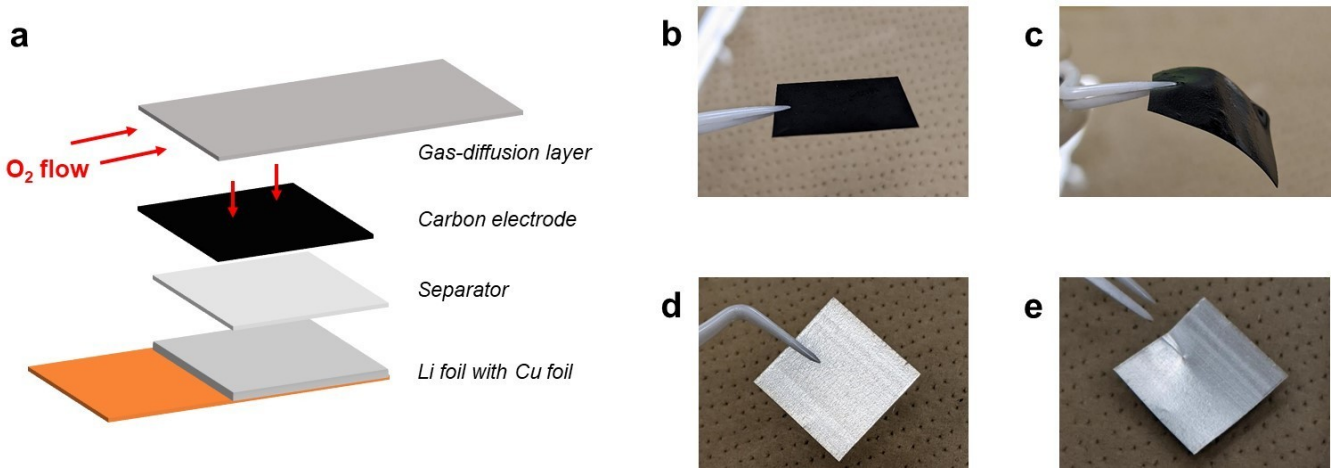

Figure 1. (a) Schematic illustration of stacked type LOB cell. Photographic images of porous carbon electrode (b) before and (c) after electrolyte injection process. Photographic images of lithium metal foil (d) before and (e) after handling by ceramic tweezers.

Research Article
doi.org/10.1002/batt.202400509
Chemistry Europe
European Chemical Societies Publishing

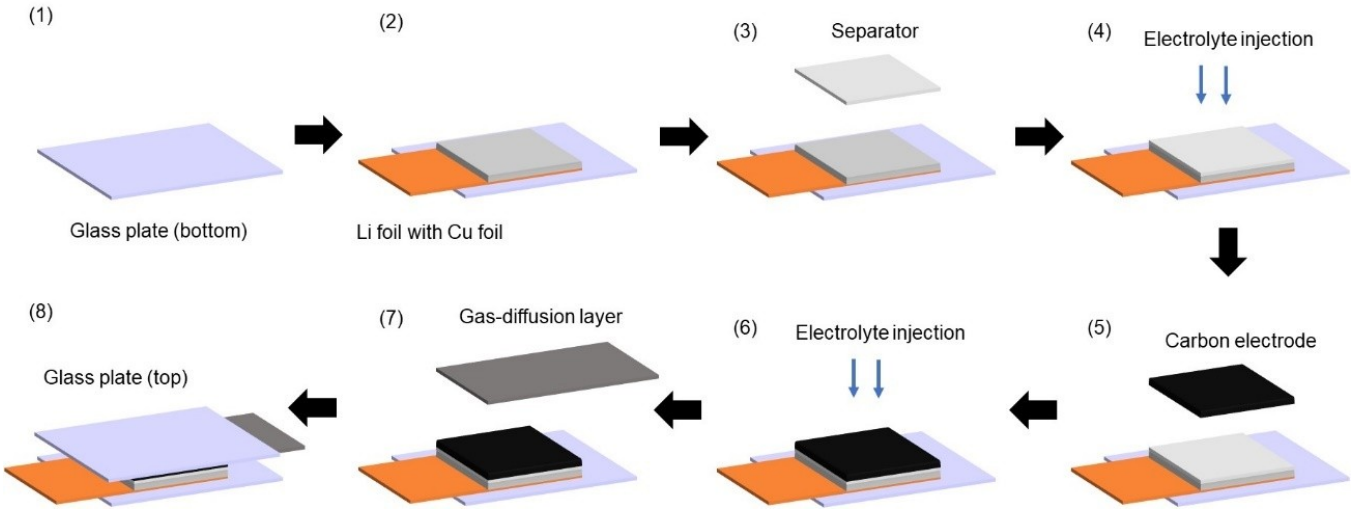

Figure 2. Schematic illustration of cell fabrication procedure by automated robotic system developed in the present study.

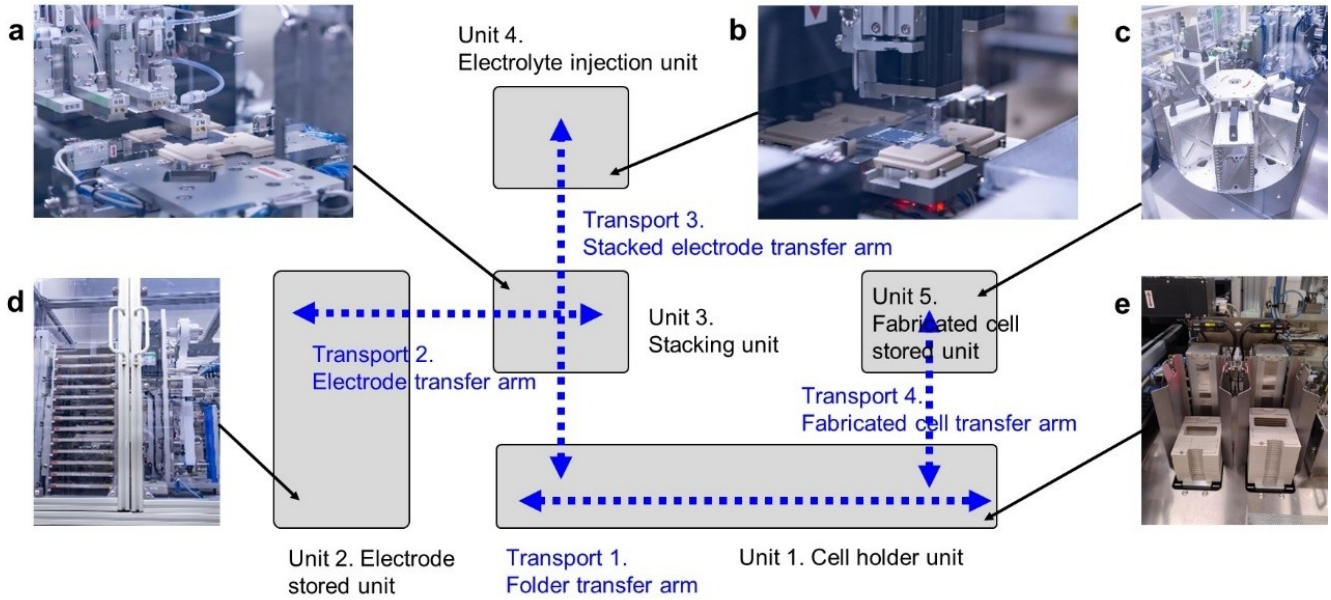

Figure 3. Photographic and schematic images of automated robotic system developed in the present study. (a) Stacking unit, (b) Electrolyte injection unit, (c) Fabricated cell stored unit, (d) Electrode stored unit, (e) Cell holder unit.

Unit 1 Cell holder unit: PEEK based cell folder (Figure S3a) is utilized for stacking LOB cells and 80 holders can be stored in cell folder unit. Glass based plate is utilized as substrate for stacking electrode materials.

Unit 2 Electrode store unit: Porous carbon membrane as positive electrode (20 mm×20 mm), lithium metal foil (20 mm×20 mm) attached with copper metal foil (20 mm×30 mm) as negative electrode, carbon fiber-based gas-diffusion layer (20 mm×30 mm) are placed on each plate and stored in the electrode uni. The separator is stored as roll and cut into individual pieces (22 mm×22 mm).

Unit 3 Stacking unit: Electrode materials are transferred from electrode storing unit to stacking unit and stacked. To minimize the damage to electrode materials, the vacuum type handling system is adopted (green line in Figure S3b). In case, electrolyte is necessary to be injected into electrode materials, cell folder is transferred to the electrolyte injection unit. For minimizing the misalignment of electrodes material during stacking and electrolyte injection process, electrode materials are holed of their edge position (red line in Figure S3b).

Unit 4 Electrolyte injection unit: Cell folder is transferred from stacking unit to electrolyte injection unit. Non-contacting type dispenser is utilized for electrolyte injection process. Inject a total of 400 droplets of electrolyte into a 20 mm×20 mm sized electrode at 1 mm intervals. The amount of one droplet of electrolyte can be quantitatively controlled.

Unit 5 Cell store unit: When all the stacking and electrolyte injection process is completed, cells are labeled their QR code and moved to cell store unit (Figure S3c). At most, 80 cells can be stored.

These five kinds of units are connected by four transport arms in following.

Transport 1 Folder transport arm: The rack at left holds plates containing positive electrodes, negative electrode and laminate sheets. A separator – the long roll of white material at right – is automatically dispensed and cut into individual pieces.

Transport 2 Electrode transport arm: The arm lifts a material from the electrode rack using a suction cup and transports it to the stacking area at the center. The suction strength of the arm is controllable, ensuring safe transfer of even extremely thin electrode materials.

Transport 3 Stacked electrode transport arm:

Transport 4 Fabricated cell transport arm: This arm transfers sealed cells to the battery cell holder.

The system developed has dimensions of approximately 5 m in length, 3 m in width, and 2 m in height, and is installed inside a dry room (Figure S3d). The cell fabrication procedure depicted in Figure 2 is executed by each unit and transport arm during specific time periods. It is important to note that by selecting appropriate electrode materials or electrolyte solutions, it is possible to create various types of LOB cells with different electrode materials and/or electrolytes. Movies for the automated cell fabrication process carried out by the developed system can be found in supporting information and elsewhere.[24]

The cell fabrication proceeds as shown in Figure 2, which consist by following eight steps. The details of cell components are described in experimental method section in Supplementary Information file.

Step 1 In Unit 1 (Cell holder unit), glass plate is placed on the top of PEEK based cell folder. Then, the cell folder is moved to Unit 3 (Stacking unit) by Transport arm 1 (Folder transport arm).

Step 2 Transport 2 (Electrode transport arm) and placed on the glass plate.

Step 3 Separator is cut into suitable size and moved to Unit 3 and placed on the Li foil.

Step 1–3 proceeds parallelly and found in Movie: 0:00–1:55.

Step 4 The cell folder is moved to Unit 4 (Electrolyte injection unit) by Transport 3 (Stacked electrode transport arm) and controlled amount of electrolyte was injected into separator (Movie: 1:56–2:57).

Step 5 The cell folder returns back to Unit 3. The porous carbon electrode is moved from Unit 2 to Unit 3 by Transport 2 and placed on the top of separator (Movie: 2:58–3:10).

Step 6 The cell folder is moved to Unit 4 and controlled amount of electrolyte was injected into porous carbon electrode (Movie: 3:11–3:46).

Step 7 The cell returns back to Unit 3. The gas-diffusion layer is moved from Unit 2 to Unit 3 by Transport 2 and placed on the top of porous carbon electrode.

Step 8 Glass plate is placed on gas diffusion layer. The cell is moved to Unit 5 by transport 1 and 4.

The developed system can fabricate one LOB cell within 10 minutes and can continuously operate to fabricate 80 cells, completing the process within 14 hours. In case, same LOB cells were fabricated by manually, it takes almost one day for fabricating the eight cells. Therefore, the developed system has a cell fabrication throughput that is 10 times higher than standard human-based experiments. In addition, the developed automated system fabricates the LOB cells with high accuracy, with an alignment error of less than 0.1 mm. This is beneficial for improving the reproducibility of battery performance tests.

To evaluate the effectiveness of the developed automated cell fabrication system, we compared the battery performance of the cell fabricated using the developed system with the cell fabricated manually. For this experiment, three independent cells were fabricated, and battery performance tests were performed at a current density of 0.4 mA/cm^2, an areal capacity of 4.0 mAh/cm^2, and a cutoff voltage of 2.0 V/4.5 V. The positive electrode utilized a KB-based self-standing membrane with a mass loading of 4.8 mg/cm^2, and the electrolyte solution contained 0.5 M LiTFSI, 0.5 M $LiNO_3$, and 0.2 M LiBr. To minimize the undesired effect of chemical crossover between electrodes, a ceramic-based separator was introduced by sandwiching it between two pieces of polyolefin-based separators. Before cycling test, the fabricated cells are firstly subjected to conditioning process, in which the cells are subjected to three repeated discharge/charge cycle with limited capacity (0.1 mAh/cm^2) and current density (0.1 mAh/cm^2), in order to improve the uniform electrolyte distribution in the cell.

Figure 4a–c shows the discharge/charge profile of LOB cells. Both manually and robotically fabricated LOB cells exhibited a representative voltage profile of LOB, consistent with previous studies using the same cell contents.[25,26] The standard deviation of the average discharge voltage and the average charge voltage was evaluated, and it was found to be less than 5 mV in both cases (Figure 4d and e). Associated with the progress of the cycle, there can be an increase in the variation of both average discharge and charge voltage. As a result, the value reached over 15 mV at the 5th cycle. In sharp contrast, for the cells fabricated by the robotic setup, the variation is less than 5 mV even at the 5th cycle. Such a difference is considered to

Research Article
doi.org/10.1002/batt.202400509
Chemistry Europe
European Chemical Societies Publishing

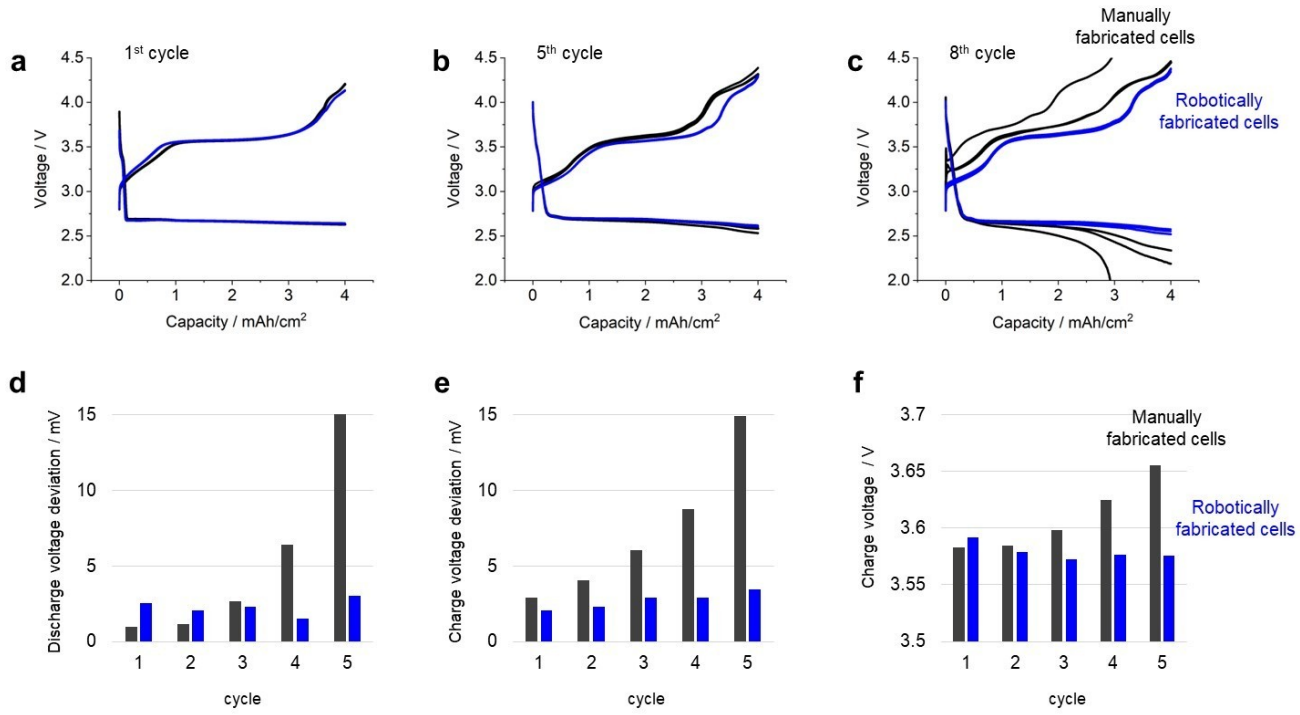

Figure 4. Voltage profile of LOB cells fabricated by manually (black curves) and by robotically (blue curves) at (a) 1st and (b) 5th, and (c) 8th cycle. Standard deviation of (d) average discharge voltage and (e) average charge voltage for LOB cells. (f) Average voltage in charge process.

originate from building quality of the cell. Namely, experimental variation factors during the cell fabrication process; mainly from the electrode alignment error, have influence of the performance variation of LOB. Notably, the other technical factors, including the amount of electrolyte and stacking pressure are essentially same for both manually and robotically fabricated LOB cells. The results demonstrate the effectiveness of the automated cell fabrication system in minimizing the validation of battery performance of LOBs, given the positional accuracy of electrode stacking of the robotic arm is less than 0.5 mm and the accuracy of electrolyte injection by the dispensing unit is less than 0.1 μL.

It should be noted that the robotically fabricated LOB cells exhibited superior battery performance compared to the manually fabricated LOB cells. In the case of the manually fabricated cells, the average charging voltage increased with each cycle and reached over 3.65 V (Figure 4f). In contrast, the average charge voltage of the robotically fabricated LOB cells remained below 3.6 V. During the 5th charging process, the robotically fabricated cells exhibited a lower voltage at the end of the process compared to the manually fabricated LOB cells. At the 8th cycle, the discharge voltage of the manually fabricated LOB cells had decreased significantly, falling below 2.5 V. On the other hand, the robotically fabricated cells exhibit a stable discharge process with a plateau of 2.6 V, revealing the novelty of the automated cell fabrication system in improving battery performance.

To demonstrate the effectiveness of the developed automated cell fabrication system in accelerating the discovery of new materials to improve the battery performance of LOB, we focus on using this setup to search for a multi-component electrolyte. In this study, we direct our research towards discovering the ideal combination of redox mediator (RM) compounds that maximize LOB performance. The use of RM is a well-known approach for improving the performance of LOBs by enhancing the Li_2O_2 decomposition reaction during the charging process.[1] In our experiment, we selected LiI, LiBr, $LiNO_3$, and TEMPO as model systems, as they are known as RM.[27–33] We manually prepared eight types of solutions listed in Table S1 and selected one to three types of solution from these eight types to mix, resulting in various kinds of electrolytes containing different combinations of RM with different concentrations. A total of 92 types of electrolytes were prepared, namely 8 C1 = 8, 8 C2 = 28, and 8 C3 = 56. These 92 cells were fabricated using a developed automated robotic system. Battery performance tests were conducted at a current density of 0.2 mA/cm^2, an areal capacity of 2.0 mAh/cm^2, and a cutoff voltage of 2.0 V/4.5 V. The ratio of electrolyte amount to areal capacity (E/C, g/Ah), which is a technological parameter of LOB, was measured. In the following cell investigation, the value of E/C is 12 g/Ah, which is relatively smaller compared to the standard LOB cell reported in the literature.[2]

Here, compared to the experiment in Figure 4, we set the half value of current density and areal capacity. Under such low E/C condition, it is reported that the sever degradation reaction proceeds in LOB cell, including the decomposition of carbon electrode and electrolyte movement phenomenon.[34,35] In the experiment in Figure 5, we set relatively mild conditions, to evaluate the influence of electrolyte composition on the LOB performance. For this experiment, we set charging cutoff

Research Article
doi.org/10.1002/batt.202400509
Chemistry Europe
European Chemical Societies Publishing

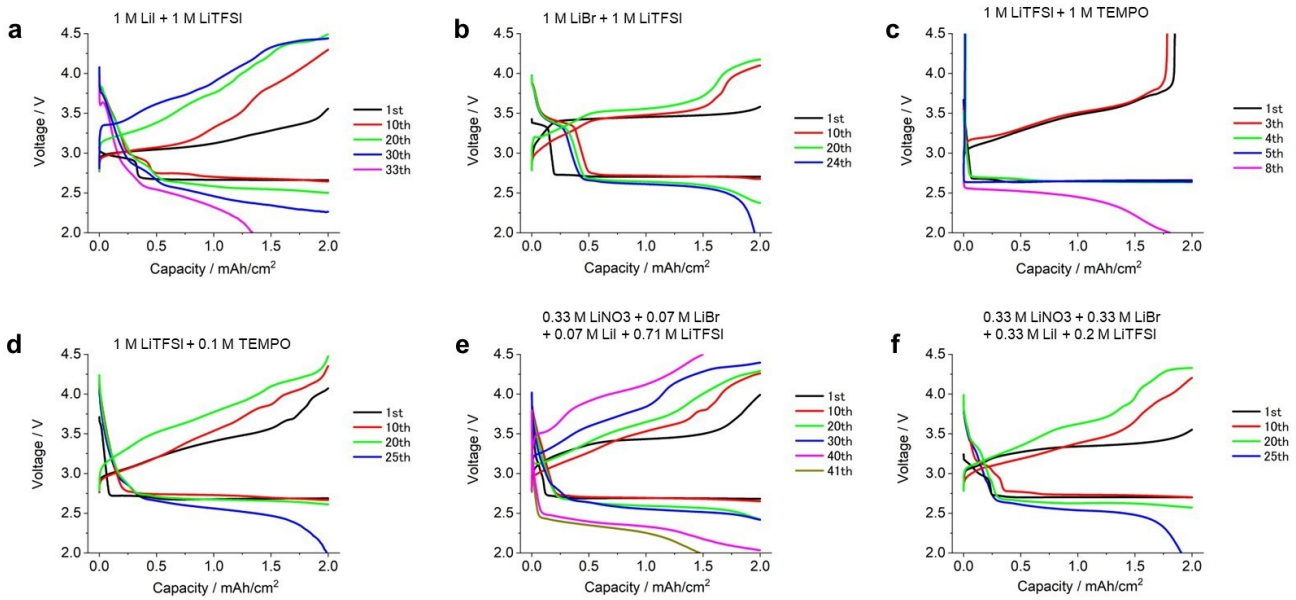

Figure 5. Voltage profile of LOB cells with electrolyte of (a) 1 M LiI + 1 M LiTFSI in TEGDME, (b) 1 M LiBr + 1 M LiTFSI in TEGDME, (c) 1 M LiTFSI + 1 M TEMPO, (d) 1 M LiTFSI + 0.1 M TEMPO in TEGDME, (e) 0.33 M $LiNO_3$ + 0.07 M LiBr + 0.07 M LiI + 0.71 M LiTFSI in TEGDME, and (f) 0.33 M $LiNO_3$ + 0.33 M LiBr + 0.33 M LiI + 0.2 M LiTFSI in TEGDME.

voltage of 4.5 V. Of course, setting lower voltage is beneficial for minimizing the oxidative side reaction that proceeds in positive electrode side. However, setting lower cutoff voltage results in the uncomplete decomposition of solid-state products (Li_2O_2 and/or Li_2CO_3) in carbon electrode.[34] As results, pore clogging of carbon electrode easily occurs, resulting in the decrease of discharge voltage. Although the details are not clarified yet, it looks, high voltage condition is necessary for fully decompose these solid products. For these reasons, in the present study we set charging cutoff voltage of 4.5 V.

Figure 5 shows the discharge/charge performance of the LOB cell with an electrolyte containing only one type of RM (8 C1). The results of cycle life of LOB cell with equipped with single kinds of RM were summarized in Table S2. When using an electrolyte with 1 M LiI + 0.2 M LiTFSI in TEGDME, the cell exhibited the typical voltage profile of LOB containing LiI (Figure 5a). During the first discharge process, there are two distinct plateaus at 2.9 V and 2.6 V. The first discharge plateau can be assigned to reduction reaction of redox couple of I^-/I_3^- and the second plateau is assigned to Li_2O_2 formation associated with the oxygen reduction reaction. During the charging process, the cell voltage increased from 3.0 V to 3.5 V, which is a typical profile of LOB containing LiI. As the cycle progressed, the charging voltage gradually increased. Finally, the cell voltage reached the cutoff voltage of 2.0 V during the 32th discharging process (purple curve in Figure 5a). During charging process when I_3^- is electrochemically generated, this I_3^- can react with Li_2O_2, generating I^- and O_2. Ideally only such reaction should proceed in the cell. However, several kinds of side reaction are reported, in which I_3^-/I^- redox involved.[36] Such side reaction is one of the reasons for increase of over-potential both in discharge/charge process with progress of cycle. When using an electrolyte with 1 M LiBr + 0.2 M LiTFSI in TEGDME, the cell exhibited the representative voltage profile of LOB containing LiBr. During the first discharge process, a two-stage plateau can be observed at 3.4 V and 2.6 V, respectively (Figure 5b). The first discharge plateau can be attributed to reduction reaction of redox couple of Br^-/Br_3^-, while the second plateau is associated with the formation of Li_2O_2 resulting from the oxygen reduction reaction. During the charging process, a voltage plateau of 3.5 V is observed. As the cycle progresses, the voltage at the end of the charging process increases, while the discharge voltage decreases. As a result, the cell voltage reached the cutoff condition of 2.0 V at the 21th discharging process. When using an electrolyte with 1 M LiTFSI + 1 M TEMPO in TEGDME, a unique voltage profile was observed. Although the cell exhibited a representative LOB voltage profile during the 1st discharge/charge cycle, there was a sharp increase in voltage during the 7th charging process (Figure 5c). The discharge voltage rapidly decreased during the 8th discharge process and reached the cutoff voltage. This charging profile has been reported in previous studies of LOB with lean electrolyte and high areal capacity conditions, and the movement of electrolytes in the carbon electrode is considered a possible mechanism.[31] In contrast, this unique charging behavior was not observed in the case of electrolyte containing 1 M LiTFSI + 0.1 M TEMPO in TEGDME (Figure 5d). The results indicate a complex degradation mechanism of LOB under low E/C conditions in the cell with electrolyte containing a high concentration of TEMPO. For clarifying the detailed mechanism of unique cell degradation phenomenon, in which the charging voltage quickly increase at the begging of charging process, the use of non-destructive analytical methods is crucial.[37] Although the understanding of such details is quite important, we recognize this is the out of scope of the present study. We believe the use of such advanced analytical techniques clarified

the unique cell degradation phenomenon observed in the present study.

The discharge and charge performance tests were also conducted on the other LOB cells using electrolytes 8 C2 and 8 C3. Figure S4 summarizes the distribution table of cycle life for all 92 LOB cells evaluated in this study, revealing an average cycle life of 28 cycles. Most cells exhibited a cycle life between the 20 and 36 cycle. Table S3 shows the details of the electrolyte composition of the top 10 samples with the highest cycle life. Of the samples investigated, the cell containing an electrolyte of 0.33 M $LiNO_3$, 0.07 M LiBr, 0.07 M LiI, and 0.71 M LiTFSI, which consists by the electrolyte No.1, No.6 and No.7, exhibited the best cycle life, lasting 41 cycles (Figure 5e). In Figure 5f, the profile of LOB cell containing an electrolyte of 0.33 M $LiNO_3$, 0.33 M LiBr, 0.33 M LiI, and 0.2 M LiTFSI, which consists by the electrolyte No. 1, No. 2 and No. 3, was also shown. Although at the beginning of cycle, the cell exhibited relatively low charging voltage, there can be seen the gradual increase of voltage with progress of cycle. At 25th discharge process, the voltage showed sudden decrease and reached to cutoff condition. Both electrolytes are consisted by four kinds of chemicals, $LiNO_3$, LiBr, LiI and LiTFSI. Only the difference is the concentration of LiBr and LiI. Notably, the LOB cell with lower RM concentration results in higher cycle life. This result suggests that the high concentration level of RM is more likely to cause new side reactions, resulting in the negative influence on the cycle life, although high concentration level of RM has positive have the positive effect of lowering the charging voltage and suppressing side reactions.

The negative effect of high concentration level RM also can be found in Table S3. Among the 10 kind of electrolyte, 9 electrolyte do not contain the solution No. 2 and No. 4, which correspond to high concentration LiBr solution and high concentration TEMPO solution. Of course, the optimum electrolyte composition can be change by the choice of battery evaluation conditions, including charging cutoff voltage, current density, areal capacity, the results obtained in the preset study revealed the existence of complicated synergetic effect of RMs. In a multi-component electrolyte system, the relationship between electrolyte composition and battery performance is complex and difficult to predict. To evaluate their performance experimentally, the use of a high-throughput experimental setup is beneficial.

Conclusions

In this study, we developed an automated robotic system for fabricating stacked-type lithium-oxygen batteries. The system can fabricate 80 LOB cells within 14 hours, which is 10 times faster than standard human-based experiments. The system also ensures high alignment accuracy during the electrode stacking and electrolyte injection processes, resulting in improved reproducibility of battery performance. To demonstrate the effectiveness of the developed system in accelerating the discovery of new materials to improve the battery performance of LOB, we attempted to identify the ideal combination of redox mediator (RM) compounds that would maximize LOB performance. Through investigation of 92 different electrolyte compositions, including various combinations of RM and their concentrations, it was determined that LOB cells with an electrolyte consisting of 0.33 M $LiNO_3$, 0.07 M LiBr, 0.07 M LiI, and 0.71 M LiTFSI exhibited the best cycle life. These results demonstrate the effectiveness of multi-component electrolyte discovery for LOB with long cycle life. The automated robotic cell fabrication technology is believed to be beneficial for accelerating the research and development of LOBs with long cycle life and high energy density.

Supporting Information Summary

Experimental details, photographic image of automated LOB cell fabrication robotic system, distribution table of cycle life of LOB cells are provided in the Supporting Information.

Acknowledgements

The present work was partially supported by JST COI-NEXT Grant Number JPMJPF2016. This work also received support from the National Institute for Materials Science (NIMS) Battery Research Platform.

Conflict of Interests

The authors declare no conflict of interest.

Data Availability Statement

The data that support the findings of this study are available from the corresponding author upon reasonable request.

Keywords: Laboratory automation · High throughput experiments · Lithium-oxygen batteries · Cell fabrication · Electrolyte

[1] W.-J. Kwak, R. D. Sharon, C. Xia, H. Kim, L. R. Johnson, P. G. Bruce, L. F. Nazar, Y.-K. Sun, A. A. Frimer, M. Noked, S. A. Freunberger, D. Aurbach, *Chem. Rev.* **2020**, *120*, 6626–6683.
[2] S. Matsuda, M. Ono, S. Yamaguchi, K. Uosaki, *Mater. Horiz.* **2022**, *9*, 856.
[3] Z. Wu, Y. Tian, H. Chen, L. Wang, S. Qian, T. Wu, S. Zhang, J. Lu, *Chem. Soc. Rev.* **2022**, *51*, 8045–8101.
[4] T. Liu, J. P. Vivek, E. W. Zhao, J. Lei, N. Garcia-Araez, C. P. Grey, *Chem. Rev.* **2020**, *120*, 6558–6625.
[5] S. Matsuda, E. Yasukawa, T. Kameda, S. Kimura, S. Yamaguchi, Y. Kubo, K. Uosaki, *Cell Rep. Phys. Sci.* **2021**, *2*, 100506.
[6] S. Matsuda, M. Ono, H. Asahina, S. Kimura, E. Mizuki, E. Yasukawa, S. Yamaguchi, Y. Kubo, K. Uosaki, *Adv. Energy Mater.* **2023**, *13*, 2203062.
[7] A. Nomura, K. Ito, Y. Kubo, *Sci. Rep.* **2017**, *7*, 1–8.
[8] J. Saengkaew, T. Kameda, S. Matsuda, *Materials Advances.* **2023**, *4*, 4417–4424.
[9] W. Yu, Z. Shen, T. Yoshii, S. Iwamura, M. Ono, S. Matsuda, M. Aoki, T. Kondo, S. R. Mukai, S. Nakanishi, H. Nishihara, *Adv. Energy Mater.* **2024**, *14*, 2303055.

[10] Y. J. Lee, S. H. Park, S. H. Kim, Y. Ko, K. Kang, Y. J. Lee, *ACS Catal.* **2018**, *8*, 2923–2934.
[11] S. Matsuda, H. Asahina, *J. Phys. Chem. C* **2020**, *124*, 25784–25789.
[12] K. Nishioka, M. Saito, M. Ono, S. Matsuda, S. Nakanishi, *ACS Appl. Energy Mater.* **2022**, *5*, 4404–4412.
[13] M. Ono, S. Matsuda, *ACS Appl. Energy Mater.* **2023**, *6*, 3357–3365.
[14] B. D. Adams, R. Black, Z. Williams, R. Fernandes, M. Cuisinier, E. J. Berg, P. Novak, G. K. Murphy, L. F. Nazar, *Adv. Energy Mater.* **2015**, *5*, 1400867.
[15] D. Sharon, P. Sharon, D. Hirshberg, M. Salama, M. Afri, L. J. W. Shimon, W.-J. Kwak, Y.-K. Sun, A. A. Frimer, D. Aurbach, *J. Am. Chem. Soc.* **2017**, *139*, 11690–11693.
[16] Z. Huang, H. Zeng, M. Xie, X. Lin, Z. Huang, Y. Shen, Y. Huang, *Angew. Chem. Int. Ed.* **2019**, *58*, 2345–2349.
[17] W. Choi, M. Kim, J. O. Park, J.-H. Kim, K. Choi, Y. S. Kim, T. Y. Kim, K. Ogata, D. Im, S.-G. Doo, Y. Hwang, *Sci. Rep.* **2017**, *7*, 12037.
[18] Y. Kubo, K. Ito, *ECS Trans.* **2014**, *62*, 129.
[19] S. Matsuda, S. Yamaguchi, E. Yasukawa, H. Asahina, H. Kakuta, H. Otani, S. Kimura, T. Kameda, Y. Takayanagi, A. Tajika, Y. Kubo, K. Uosaki, *ACS Appl. Energy Mater.* **2021**, *4*, 2563–2569.
[20] H. C. Lee, J. O. Park, M. Kim, H. J. Kwon, J. H. Kim, K. H. Choi, K. Kim, D. Im, *Joule* **2019**, *3*, 542–556.
[21] J. O. Park, M. Kim, J. H. Kim, K. H. Choi, H. C. Lee, W. Choi, S. B. Ma, D. Im, *J. Power Sources* **2019**, *419*, 112–118.
[22] S. Zhao, L. Zhang, G. Zhang, H. Sun, J. Yang, S. Lu, *J Energy Chem.* **2020**, *45*, 74–82.
[23] J. W. Jordan, G. Vailaya, C. Holc, M. Jenkins, R. C. McNulty, C. Puscalau, B. Tokay, A. Laybourn, X. Gao, D. A. Walsh, G. N. Newton, P. G. Bruce, L. R. Johnson, *Faraday Discuss.* **2024**, *248*, 381–391.
[24] https://youtu.be/ Me6qHyJYwa0 .
[25] M. Ue, H. Asahina, S. Matsuda, K. Uosaki, *RSC Adv.* **2020**, *10*, 42971–42982.
[26] M. Ono, S. Matsuda, *J. Phys. Chem. C* **2023**, *127*, 6117–6124.
[27] X. Xin, K. Ito, Y. Kubo, *ACS Appl. Mater. Interfaces* **2017**, *9*, 25976–25984.
[28] S. Matsuda, G. Lambard, K. Sodeyama, *Cell Rep. Phys. Sci.* **2022**, *3*, 100832.
[29] H. D. Lim, H. Song, J. Kim, H. Gwon, Y. Bae, K. Y. Park, J. Hong, H. Kim, T. Kim, Y. H. Kim, X. Leprõ, R. Ovalle-Robles, R. H. Baughman, K. Kang, *Angew. Chem. Int. Ed.* **2014**, *53*, 3926–3931.
[30] Z. Liang, Y.-C. Lu, *J. Am. Chem. Soc.* **2016**, *138*, 7574–7583.
[31] D. Sharon, D. Hirsberg, M. Afri, F. Chesneau, R. Lavi, A. A. Frimer, Y.-K. Sun, D. Aurbach, *ACS Appl. Mater. Interfaces* **2015**, *7*, 16590–16600.
[32] B. J. Bergner, A. Schürmann, K. Peppler, A. Garsuch, J. Janek, *J. Am. Chem. Soc.* **2014**, *136*, 15054–15064.
[33] B. J. Bergner, M. R. Busche, R. Pinedo, B. B. Berkes, D. Schröder, J. Janek, *ACS Appl. Mater. Interfaces* **2016**, *8*, 7756–7765.
[34] M. Ono, J. Saengkaew, S. Matsuda, *Adv. Sci.* **2023**, *10*, 2300896.
[35] S. Matsuda, E. Yasukawa, S. Kimura, S. Yamaguchi, K. Uosaki, *Faraday Discuss.* **2024**, *248*, 341–354.
[36] W. J. Kwak, D. Hirshberg, D. Sharon, H. J. Shin, M. Afri, J. B. Park, A. Garsuch, F. F. Chesneau, A. A. Frimer, D. Aurbach, Y. K. Sun, *J. Mater. Chem. A* **2015**, *3*, 8855–8864.
[37] S. Matsuda, S. Kimura, K. Uosaki, *J. Phys. Chem. C* **2023**, *127*, 11822–11828.

Manuscript received: July 29, 2024
Revised manuscript received: September 3, 2024
Accepted manuscript online: September 6, 2024
Version of record online: October 28, 2024